The Journal of Experimental Biology 203, 2247–2259 (2000)
Printed in Great Britain © The Company of Biologists Limited 2000
JEB2618

LOCOMOTION IN SCOMBRID FISHES: MORPHOLOGY AND KINEMATICS OF THE FINLETS OF THE CHUB MACKEREL *SCOMBER JAPONICUS*

JENNIFER C. NAUEN*,‡ AND GEORGE V. LAUDER*

Department of Ecology and Evolutionary Biology, University of California, Irvine, CA 92697, USA

*Present address: Department of Organismic and Evolutionary Biology, Harvard University, Cambridge, MA 02138, USA
‡e-mail: jnauen@oeb.harvard.edu

Accepted 5 May; published on WWW 10 July 2000

Summary

Finlets are small non-retractable fins located on the dorsal and ventral margins of the body between the second dorsal and anal fins and the tail of scombrid fishes. The morphology of the finlets, and finlet kinematics during swimming in a flow tank at speeds of 0.8–3.0 fork lengths s^{-1}, were examined in the chub mackerel *Scomber japonicus*. Functionally, *S. japonicus* has five dorsal and anal triangular finlets (the fifth finlet is a pair of finlets acting in concert). Slips of muscle that insert onto the base of each finlet indicate the potential for active movement. In animals of similar mass, finlet length and area increased posteriorly. Finlet length, height and area show positive allometry in animals from 45 to 279 g body mass. Summed finlet area was approximately 15 % of caudal fin area.

During steady swimming, the finlets typically oscillated symmetrically in the horizontal and vertical planes. Finlet excursions in the *x*, *y* and *z* directions ranged from 1 to 5 mm, increased posteriorly and were independent of speed. The timing of the maximum amplitude of oscillation was phased posteriorly; the phase lag of the maximum amplitude of oscillation was independent of speed. During some periods of gliding, a finlet occasionally moved independently of the body and the other finlets, which indicated active control of finlet movement.

The angle of attack of the finlets averaged approximately 0 ° over a tailbeat, indicating no net contribution to thrust production *via* classical lift-based mechanisms. However, the timing of finlet movement relative to that of the tail suggests that more posterior finlets may direct some flow longitudinally as the tail decelerates and thereby contribute flow to the developing caudal fin vortex.

Movies available on-line:
http://www.biologists.com/JEB/movies/jeb2618.html

Key words: locomotion, swimming, scombrid fish, kinematics, finlets, mackerel, *Scomber japonicus*.

Introduction

Scombrid fishes (mackerels, bonitos and tunas) are noted for their high-performance locomotion. These fishes are capable of relatively high burst speeds [from 18 *BL* s^{-1}, where *BL* is body length, for mackerel (Wardle and He, 1988) to 27 *BL* s^{-1} for tuna (Fierstine and Walters, 1968; also see Magnuson, 1978)] and high cruising speeds [from 3.5 *BL* s^{-1} for mackerel (Wardle and He, 1988) to 6–10 *BL* s^{-1} for tuna (Yuen, 1970; summarized in Beamish, 1978)]. In addition, scombrids are known to migrate long distances (as far as 9700 km for the trans-Pacific crossing of the bluefin tuna; Lindsey, 1978). The morphology and kinematics of scombrids, especially in relation to hydrodynamic efficiency and energetics, have been the subject of numerous studies (e.g. Walters, 1962; Magnuson, 1970; Westneat et al., 1993; Dewar and Graham, 1994; Blake et al., 1995; Gibb et al., 1999).

Finlets are among the more unusual of the morphological specializations of scombrid fishes. These small, non-retractable fins are situated on the dorsal and ventral body margin and span the region between the second dorsal and the anal fins and the caudal peduncle (Fig. 1). Scombrid fishes have 5–12 finlets (Collette and Nauen, 1983). On the basis of a phylogeny by Block et al. (1993), the range in finlet number is similar in primitive and advanced scombrid species (Fig. 1).

The ubiquity of finlets in the high-performance scombrid fishes (Fig. 1) and the position of the finlets immediately anterior to the caudal fin suggest that finlets play a role in locomotion. Walters (1962) proposed that the finlets direct flow longitudinally along the body and prevent roll. Lindsey (1978) postulated that the finlets deflect water across the caudal peduncle and enhance locomotory performance by preventing separation of the boundary layer and thus reducing drag. Magnuson (1970) proposed that the finlets direct water across the pronounced central caudal keel of tuna and thereby contribute to any lift forces produced at the keel. Aleev (1969) and Helfman et al. (1997) hypothesized that the finlets eliminate or prevent vortices in water shed from the median fins and thus provide a less turbulent environment for oscillation of the tail.

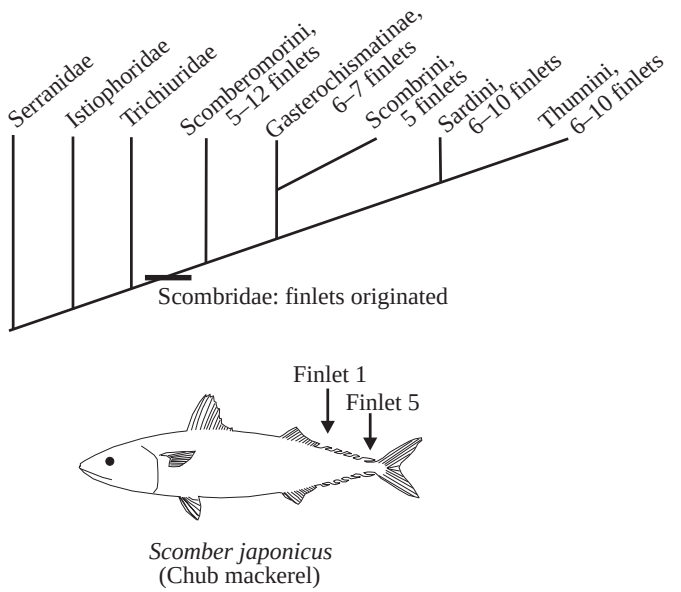

Fig. 1. Phylogeny of scombrid fishes, based on Block et al. (1993), with finlet numbers from Collette and Nauen (1983). The chub mackerel *Scomber japonicus* (a member of the Scombrini) functionally has five finlets (see Fig. 2), labeled here from 1 to 5 anteriorly to posteriorly.

The size and scaling of finlets, and the magnitude and timing of their movement relative to each other and to the tail, are factors relevant to understanding the locomotory function of finlets. However, there are no data on finlet morphology or on their movements during locomotion. The aim of this paper is to provide the first data on the morphology, scaling and kinematics of the finlets of a representative scombrid fish, the chub mackerel *Scomber japonicus*. These data will be used to evaluate the above-mentioned hypotheses of finlet function and to outline future experiments on the hydrodynamics of the finlets, caudal peduncle and caudal fin of scombrid fishes.

Materials and methods

Animals

Chub mackerel, *Scomber japonicus* (Houttuyn), were collected by fishing from various locations in coastal southern California, USA. The animals were fed chopped smelt and housed in 1200 l tanks at a water temperature of 18±2 °C in a photoperiod of 12 h:12 h light:dark. Seven individuals ranging in fork length (L) from 18 to 27 cm were used for kinematic studies. Additional specimens (fresh, frozen and preserved) were used for morphological studies.

Morphology

Morphological measurements were only made on specimens hand-caught using a hook and line and transported by us to the laboratory because the finlets are easily damaged by handling. Specimens purchased from local markets could not be used because the finlets were usually damaged and were occasionally missing completely. To measure finlet length, height and area, specimens were viewed using a Javelin CCD camera. Images were imported into a PC computer and digitized using a custom-designed digitizing program. Two of the specimens used in the kinematic study were killed, sectioned anterior to the second dorsal fin, and cleared and stained using techniques described by Dingerkus and Uhler (1977).

Kinematics of the finlets

Experiments were conducted using a calibrated 600 l flow tank with a working area 82 cm long, 28 cm wide and 28 cm high at 19±1 °C. Flow speed in the tank was controlled using a variable-speed motor (details of the flow tank and calibration have been presented previously; see, for example, Jayne et al., 1996; Gibb et al., 1999). Use of the flow tank and a magnified field of view (4 cm×4 cm) on the cameras allowed us a clear view of the finlets, which are of the order of 1 cm in length, for a series of sequential tailbeats.

Two cameras were aimed perpendicular to the flow tank. The first camera was focused on a front-surface mirror immersed in the flow at an angle of 45 ° to the *xz* plane. This mirror showed a dorsal view of the fish. The second camera was focused in the lateral (*xy*) plane to give a lateral view of the fish. The lateral and dorsal camera views were scaled equally at the start of the experiment using two rulers oriented perpendicular to each other. When an animal was in the field of view of the cameras and the image was in focus, the animal was swimming in the center of the working section of the flow tank. The two cameras were part of a NAC HSV500 high-speed video system that collected synchronous images at 250 Hz.

Three individuals (fork length, L=23.9±2.2 cm, mean ± S.D.) were videotaped using a NAC HSV500 high-speed video system. Video images were collected at steady swimming speeds of 1.2, 1.6, 2.2 and 3 $L\,s^{-1}$. These speeds are within the range of swimming speeds (0.4–3.5 body lengths s^{-1}) that mackerel can sustain for more than 200 min (Wardle and He, 1988). Four to six sequential tailbeats were analyzed for each individual at each speed. A fourth individual (L=22 cm) was filmed at low speeds (<1 $L\,s^{-1}$) to examine the kinematics of finlets during periods of gliding.

Images were imported into the computer using the BUZ video system (Iomega) and digitized using the NIH image software program (developed at the National Institute of Health, USA). The three-dimensional orientation of individual finlets was not determined because the images lacked sufficient resolution at this level of magnification for detailed three-dimensional analysis. Preliminary video recordings showed that the finlets are relatively stiff and that finlet structure and movement could be approximated as flat plates that pivot and dip around their anterior insertion point. Therefore, to quantify finlet movement we digitized three parameters. From the dorsal-view images, we digitized the angle between the finlets and the body midline (β) and a point at the anterior base of the most posterior finlet in the field of

view (as an index of body undulation). From the lateral-view images, we digitized the maximum vertical (*y*) excursion of the finlets.

The time series data were filtered for the high-frequency noise that is inherent in digitized data (Biewener and Full, 1992) using Acknowledge software (BIOPAC Systems). Spectrum analysis of the data using a Fourier transform revealed the primary frequency of the time series; the cut-off value for the high-pass filter was set at five times the primary frequency of the data. Analysis of the β values for one individual (*L* 22 cm) at four speeds indicated that, on average, this filtering protocol altered data values by less than 2° (1.6±1.2°, mean ± S.D., *N*=542) and did not contribute phase shifts to the data.

The maximum *x* and *z* excursions of the tip of each finlet were calculated trigonometrically from the β values using finlet length. Because only the left side of the fish was visible in the *xy* plane, and the posterior tips of the finlets were hidden behind the body for half the tailbeat, approximately twice as much data were collected for the *x* and *z* excursions as for the *y* excursions. Phase lag was calculated as the proportion of the tailbeat cycle to maximum β values. The caudal fin was not in the field of view of these images, so tailbeat cycle was determined by digitizing the insertion point of the most posterior finlet in the field of view.

Angle of attack of the finlets and tail

The tail was not visible in the close-up images of the finlets recorded with the NAC HSV500 (see Fig. 5), so three other individuals (*L*=19.4±0.5 cm, mean ± S.D.) were filmed at 250 fields s^{-1} using a second video system, the NAC HSV 500 C^3. The camera and mirror were set up as described above with a field of view of 8 cm×4 cm so that the finlets and tail were viewed simultaneously.

Because our kinematic data indicated no effect of speed on the magnitude and timing of finlet movements (detailed in the Results section), α values for finlets 3, 4 and 5 were determined for the single speed of 2.2 *L* s^{-1} (three tailbeats for each individual); α was calculated as the path angle minus the orientation angle θ (Jayne et al., 1996; Gillis, 1997). The path angle is the angle between the direction of forward travel and a straight line connecting the midpoint of the structure at time 1 to the midpoint of the structure at time 2; θ is the angle between the structure and the direction of forward travel (see Fig. 4 in Gillis, 1997). Using the methods described above, video images were imported into the computer, and the midpoint of the length of each finlet and the tail, θ, and a point on the caudal peduncle (an index of tail movement) were digitized from the *xz* view. The path angle was calculated trigonometrically. Values of path angle and θ were filtered as described above, and α values were calculated for the finlets and the tail. Note that this method of calculating α assumes that the direction of travel represents the direction of the local water flow; this assumption was not tested here because flow visualization methods were not used.

The speed of the caudal peduncle was calculated from the filtered position data as:

$$S_t = (x_{t+i} - x_{t-i})/(2\Delta t), \quad (1)$$

where S_t is speed at time *t* and x_{t+i} and x_{t-i} are the positions of the caudal peduncle at times *t*+i and *t*–i, respectively (Winter, 1989). Acceleration was calculated by substituting *S* for *x* in equation 1. The method of Winter (1989; also see Nauen and Shadwick, 1999) produced virtually identical speed and acceleration data to those generated using the quintic spline method in the QuickSAND program (Walker, 1998). The quintic spline method was generally recommended by Walker (1998) in his comparison of numerical differentiation algorithms for calculating velocity and acceleration values. In this paper, we present speed and acceleration data in a manner designed to facilitate comparison among tailbeat cycles. Thus, speed rather than velocity was calculated, which omitted the direction of travel information from the acceleration data.

Statistical analyses

Statistical analyses were performed using Statgraphics (version 3.0 for Windows, STSC, USA) and SuperANOVA (version 1.11 for the Macintosh). Statistical probability was established at the $P \leqslant 0.05$ level unless stated otherwise.

Scaling relationships of morphological characteristics were analyzed in relation to animal size (represented by fork length, *L*). Statistical comparisons of the slopes were made using Statgraphics. The reduced-major-axis (RMA) regression model was used to calculate the scaling relationships because it does not assume that the values of *x* (*L* in this case) are determined without error [an assumption made in ordinary least-square regression (OLS) models]. The RMA equation is $y=b_0+b_1x$, where b_0 is the *y*-intercept and b_1 is the slope (Davis, 1986). The slope is equal to the standard deviation of *y* divided by the standard deviation of *x*; the *y*-intercept was calculated from the above equation. The standard error of the RMA slope is equal to the standard error of the slope calculated for an OLS model (LaBarbera, 1989).

The angle and phase data for finlets 3, 4 and 5 were each analyzed as a three-way analysis of variance (ANOVA) in which speed and finlet number were considered fixed effects and individual was considered a random effect. *F*-values were calculated as described by Zar (1984). A multivariate ANOVA could not be performed on the *x*, *y* and *z* excursion data because of insufficient degrees of freedom; therefore, each parameter was separately analyzed using a three-way ANOVA with effect and error terms as described above. The α data were analyzed as a three-way ANOVA in which tail position and structure (finlets 3–5 and the tail) were considered fixed effects and individual was considered a random effect. Tukey–Kramer *post-hoc* tests were performed on each variable that showed significant effects of speed, finlet number or structure.

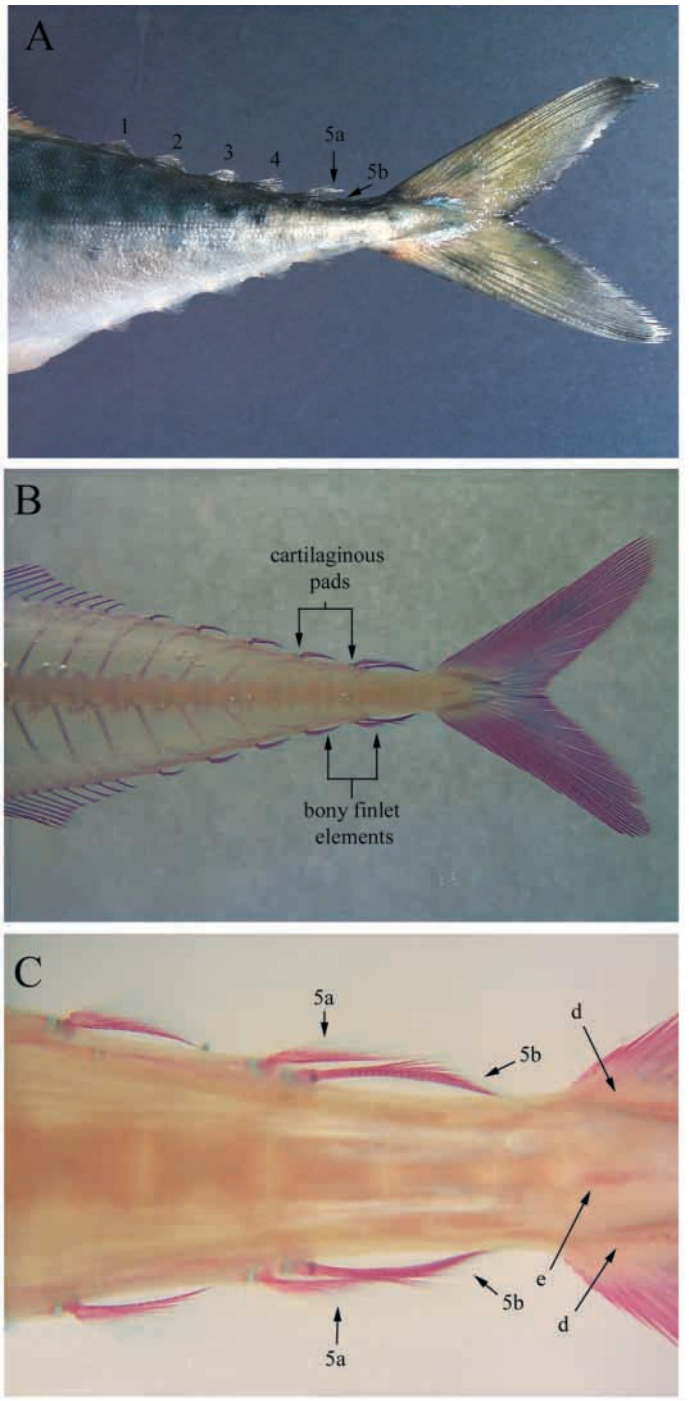

Fig. 2. A lateral view of the dorsal and ventral finlets, peduncle and tail of a fresh specimen (23 cm fork length, A) and a cleared and stained specimen (23.5 cm, B) of *Scomber japonicus*. The finlets are labeled 1–5 anteriorly to posteriorly (shown for the dorsal finlets, A). Each finlet is covered by an extremely thin, clear membrane. The finlets contain bony elements (stained red, B) which articulate on a cartilaginous pad (stained blue, B). The fifth finlet (A,B,C) consists of two separate groups of bony and soft tissue elements (finlets 5a and 5b, C) ,which are bound by the clear membrane and function as a single finlet. Two lateral caudal keels (d) and one central keel (e) are posterior to the finlets on the caudal peduncle (C).

Results

Description and scaling of morphology

The shape of the finlets approximates an elongated obtuse triangle (Fig. 2). A clear membrane that is easily disrupted covers each finlet (this membrane is often destroyed on specimens that have been handled or frozen). A series of bony jointed fin rays (Fig. 2B,C) stiffens each finlet. These rays expand at the anterior base into an articulation associated with a cartilaginous pad (Fig. 2B,C). The cartilaginous pad is associated with a pterygiophore. The base of each finlet is associated with two tendons; these tendons are each attached to a bundle of muscle fibers. Pulling on these muscles with a pair of forceps results in posterior or lateral movement of the associated finlet, which suggests that finlet movement could be actively controlled. These finlet muscles appear to be homologous to the inclinator, depressor and erector muscles of the dorsal fin. The structure labeled finlet 5 is actually two finlets that are externally bound together by a clear membrane (Fig. 2C). With disruption of the membrane, each of these finlets (labeled posteriorly as 5a and 5b, respectively) can be manipulated separately. Finlets 5a and 5b each articulate on a separate cartilaginous pad (Fig. 2C). Separate tendon and muscle bundles insert at the base of both of finlets 5a and 5b. Finlet 5a is similar in shape to finlets 1–4, but finlet 5b is more flattened and elongated.

Posterior to finlet 5 are two lateral (d in Fig. 2C) caudal keels which each consist of a series of fine, short bony elements (possibly modified scales). Both the dorsal and ventral lateral keel are posteriorly oriented towards the body midline and extend to approximately the middle of the tail. The central caudal keel structure (e in Fig. 2C) is a single bony element that is visible under the skin in cleared and stained specimens but does not project above the body surface.

In three individuals of similar mass (84.7±0.6 g, mean ± S.D.), dorsal and ventral finlets 1–4 were very similar in length and height (Fig. 3). Finlet area (which was measured by digitizing the finlet shape, not calculated from length and height measurements) tended to be larger for the ventral finlets than for the dorsal finlets (Fig. 3). On the basis of finlet number, ANOVA indicated no significant difference in finlet height (P<0.42), but significant differences in finlet length (P<0.001) and area (P<0.001). *Post-hoc* tests indicated that finlet length increased posteriorly: the lengths of the dorsal and ventral finlets 5 were significantly different from those of the other four finlets (although dorsal finlet 5 was not significantly different in length from ventral finlet 4). Finlet area was significantly different on the basis of finlet number (P<0.05). Finlet area tended to increase posteriorly (Fig. 3), although the fifth finlets were not significantly different from the other four finlets. Summed finlet area was 15±6 % (mean ± S.D., N=14) of caudal fin area; this percentage was independent of fish size.

Statistical comparison of regression models fitted to the length data for each of the 10 finlets indicated that there were

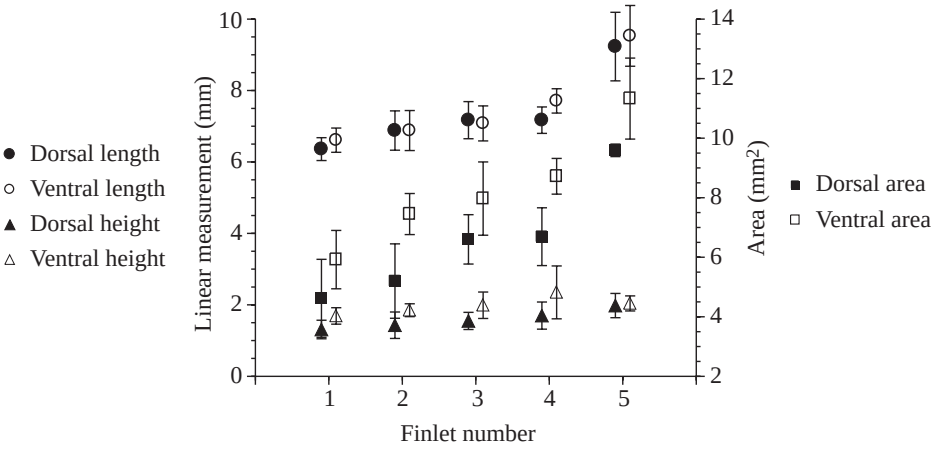

Fig. 3. The length (circles), height (triangles) and area (squares) of the dorsal (filled symbols) and ventral (open symbols) finlets from three individuals of similar mass (84.7±0.6 g, mean ± S.D.). Values are means ± S.D., *N*=3.

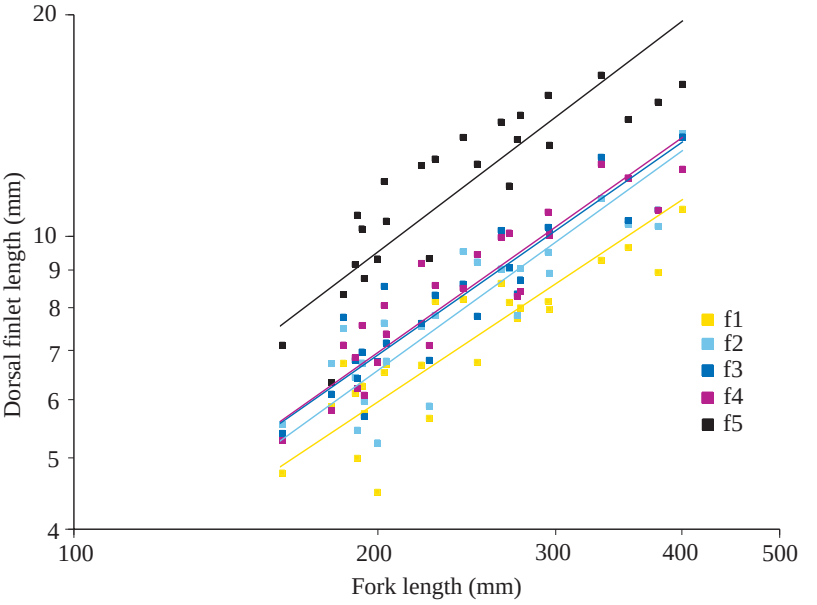

Fig. 4. Scaling of the length of dorsal finlets 1 (f1, yellow), 2 (f2, light blue), 3 (f3, dark blue), 4 (f4, purple) and 5 (f5, black). The lines are reduced-major-axis regression models fitted to the data. The slopes of the regression models for the different finlets were not significantly different. Significant differences in the *y*-intercepts reflect the posterior increase in finlet length (Fig. 3). See Table 1 for the scaling data for all the finlets.

no significant differences in slope (P<0.83, Fig. 4), although there were significant differences in the *y*-intercepts (P<0.00001, Fig. 4). The result was the same for finlet height and area (P<0.72 for the slopes and P<0.0001 for the *y*-intercepts of both of the height and area models). The significant differences in *y*-intercept values reflect the tendency of finlet length to increase posteriorly (Fig. 3) and the larger length and area of dorsal and ventral finlet 5 (Fig. 3). Given the lack of significant differences among the slopes of the models fitted to data from individual finlets, the data for each finlet parameter were grouped, and a single RMA regression model was applied to calculate the overall slope (Table 1). These slopes were compared with the isometric expectation using a *t*-test (P=0.05). The significant differences between the isometric values and the scaling relationships for length, height and area (Table 1) indicate that the finlets exhibit slight positive allometry with growth.

Table 1. *Scaling of finlet morphology as a function of fork length*

Finlet parameter	Isometric slope value	Slope ± S.E.M.	Standard error of the estimate	r^2	N‡
Length	1	1.16±0.05*	0.09	0.52	248
Height	1	1.28±0.06*	0.10	0.49	249
Area	2	2.19±0.09*	0.15	0.59	247

Slopes are calculated using reduced-major-axis regression models fitted to pooled data from dorsal and ventral finlets 1–5 for 25 animals ranging from 45 to 279 g in body mass and from 161 to 295 mm in fork length.

S.E.M., standard error of the slope estimate. The standard error of the estimate is the standard deviation of the residuals and can be used to construct prediction limits for new observations.

*These slopes are significantly different from isometric values.

‡For three animals, either the length or the height (and thus area) could not be measured for one of the finlets.

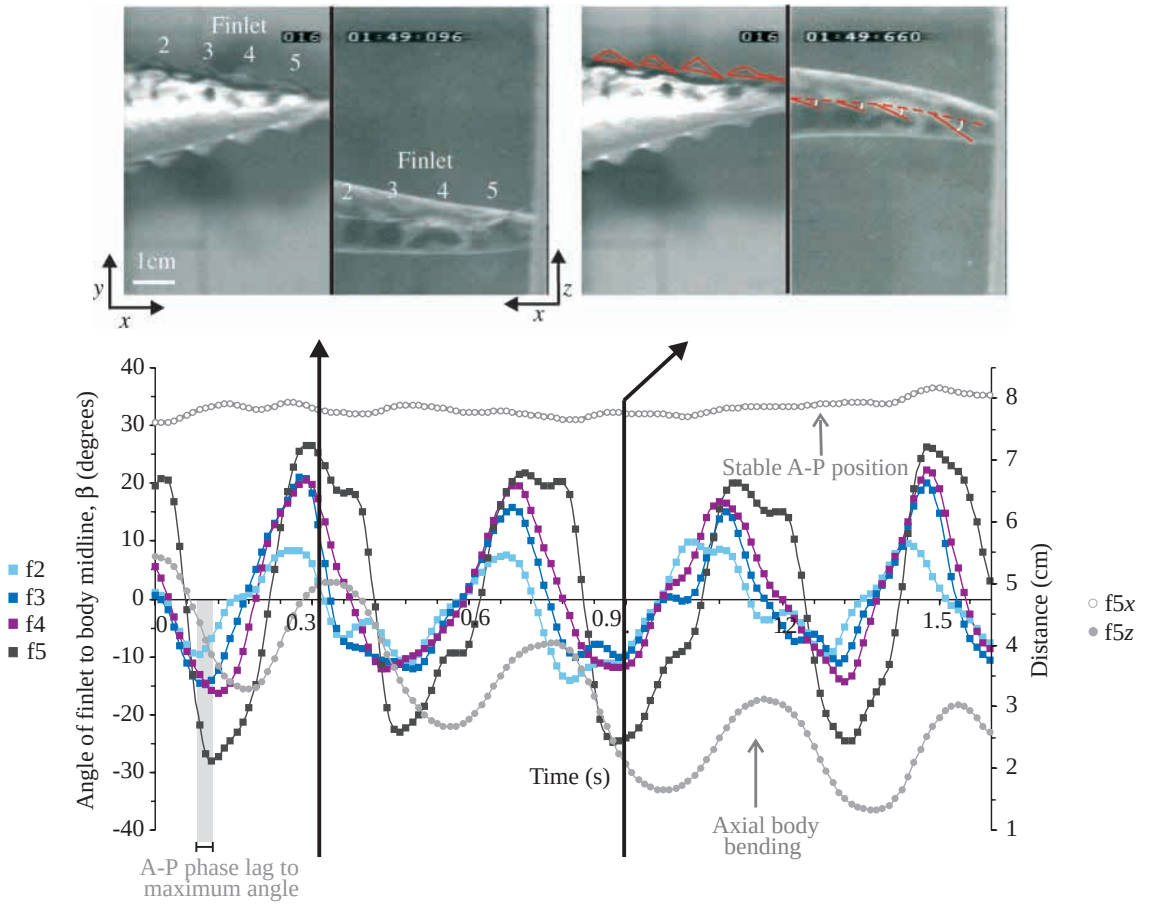

Fig. 5. A representative time series of the angle relative to the body midline (β) of finlets 2 (f2, light blue), 3 (f3, dark blue), 4 (f4, purple) and 5 (f5, black) for a 26.5 cm fish swimming steadily at 1.2 $L\,s^{-1}$, where L is fork length. The positive and negative values of finlet angle indicate movement to the left and right side of the body midline, respectively. The dorsal finlets are outlined in red in the lateral view of the second set of images on the right; the dorsal view of that set shows how the angle (β) between the finlets (solid red lines) and the body midline (dotted red line) was determined. The arrows on the time series indicate the time point of the images. Steady swimming is indicated by the stable anteroposterior (A-P) position of the body (open circles) in the 4 cm×6 cm field of view, and the symmetrical and consistent axial body bending (indicated by the undulating anteroposterior position of finlet 5 on the *z* axis; gray circles).

Table 2. *Results (*F*-values) of the three-way ANOVAs on the maximum value of β, the phase lag of maximum β and the maximum* x, y *and* z *excursions of finlets 3, 4 and 5*

Variable	Individual	Finlet number	Individual × speed	Individual × finlet	Individual × speed × finlet
d.f.	2, 308	2, 6	6, 308	4, 308	12, 308
β_{max}	29.3	70.7	13.2	–	–
Phase lag	30.5*	26.7	–	–	–
x	35.3	350.6	17.3	–	3.0
y	16.2‡	9.5	2.5‡	10.1‡	3.6‡
z	58.9	254.4	12.2	2.5	–

β is the angle between the finlet and the body midline.

d.f. is the degrees of freedom.

Only the statistically significant effects ($P<0.05$) are shown. Since speed and finlet × speed terms had no significant *F*-values for any variable, they have been omitted from this table.

*In this case, d.f. for the error term equals 262.

‡In these cases, d.f. for the error term equals 133.

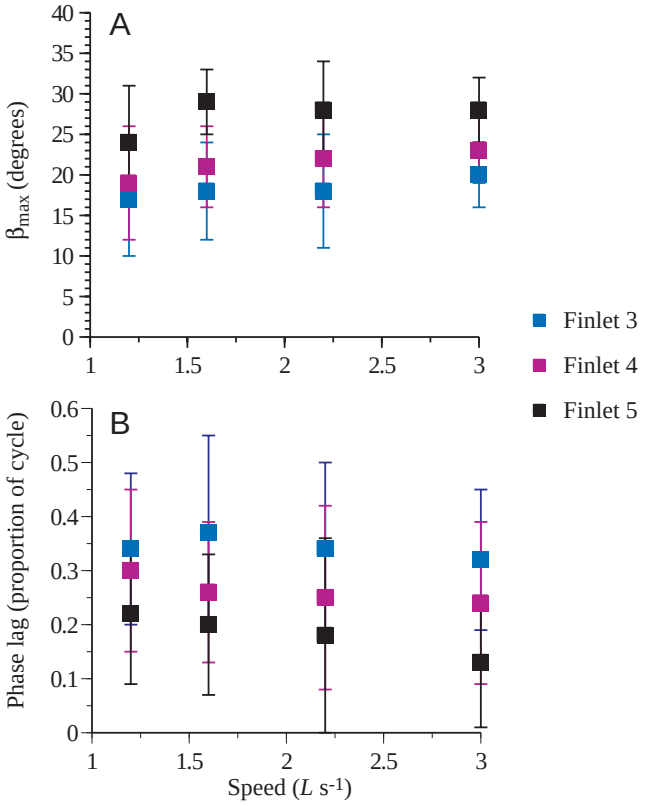

Fig. 6. The maximum angle of the finlets to the body midline (β_{max}, A) and the phase lag between β_{max} and the maximum amplitude of oscillation of the body at finlet 5 (proportion of cycle, B) as a function of swimming speed. Data for three individuals are grouped in these graphs to illustrate the lack of a significant speed effect, although a three-way ANOVA indicated significant differences among individuals for both variables, and significant individual×speed effects for β_{max} values (Table 2). Values are means ± S.D., N=22–38. L is fork length.

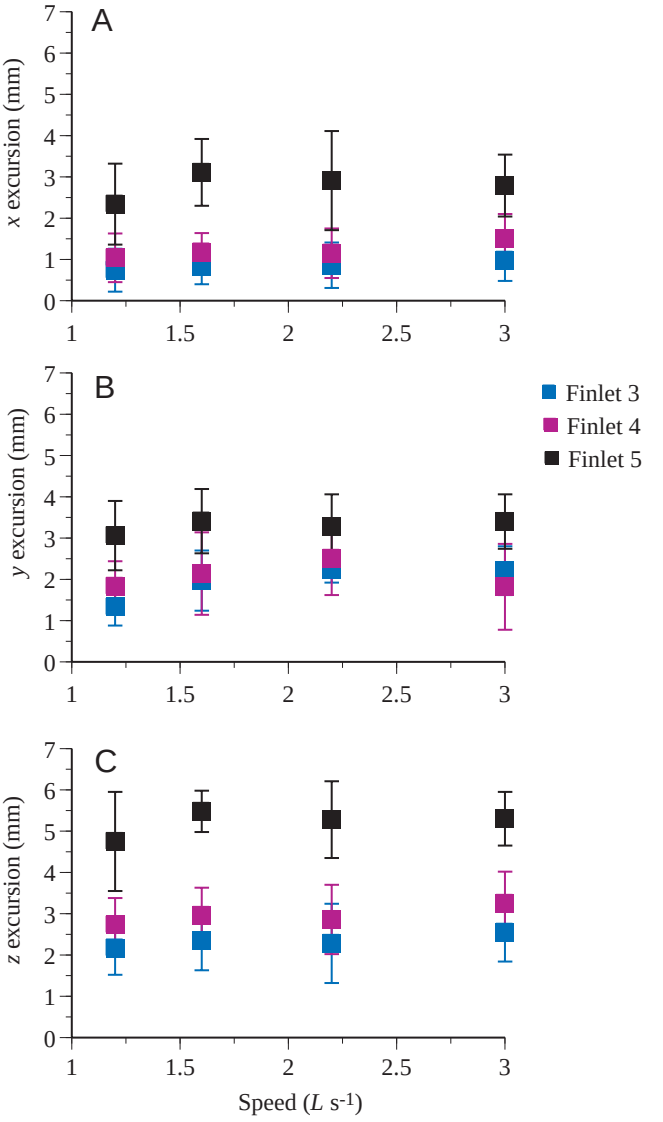

Fig. 7. The maximum x (A), y (B) and z (C) excursions of the posterior tips of finlets 3 (blue), 4 (purple) and 5 (black) as a function of swimming speed. The data for three individuals are grouped here to illustrate the absence of speed effects, although the x, y and z displacements showed significant differences among individuals (Table 2). Values are means ± S.D., N=23–38 for x and z; N=9–19 for y. L is fork length.

Kinematics during steady swimming

The time series of the angle of the finlet to the body midline (β, Fig. 5) indicated that during steady swimming the finlets oscillated symmetrically around the body midline. In addition, these data suggested that the amplitude of finlet oscillation in the z direction increased posteriorly and that maximum finlet displacement in the z direction occurred first anteriorly and then sequentially in finlets 2–5.

The ANOVA of maximum finlet oscillation amplitude (quantified as maximum values of β, β_{max}) as a function of individual, speed and finlet indicated that there were significant differences in the data due to individual (P<0.0001), finlet (P<0.008) and individual×speed effects (P<0.0001), but no significant speed or speed×finlet interaction (Table 2; Fig. 6A). The significant individual×speed effect indicates that the three individuals did not show consistent changes in β_{max} with increased speed. The *post-hoc* test indicated that the maximum amplitudes of finlets 3, 4 and 5 were significantly different from each other.

The ANOVA of the phase lag of the maximum amplitude of oscillation as a function of individual, speed and finlet indicated that the phase lag was independent of speed (P<0.47, Fig. 6B), but there were significant differences in the data due to individual (P<0.0001) and finlet (P<0.0048, Table 2) effects. The phase lags of finlets 3, 4 and 5 were all significantly different from each other.

The three ANOVAs of the x, y and z excursion data indicated that all three data sets showed individual, finlet and individual×speed effects, but no significant speed or speed×finlet interactions (Table 2). In addition, excursions in the x and y directions showed individual×speed×finlet effects, and excursions in the y and z directions showed

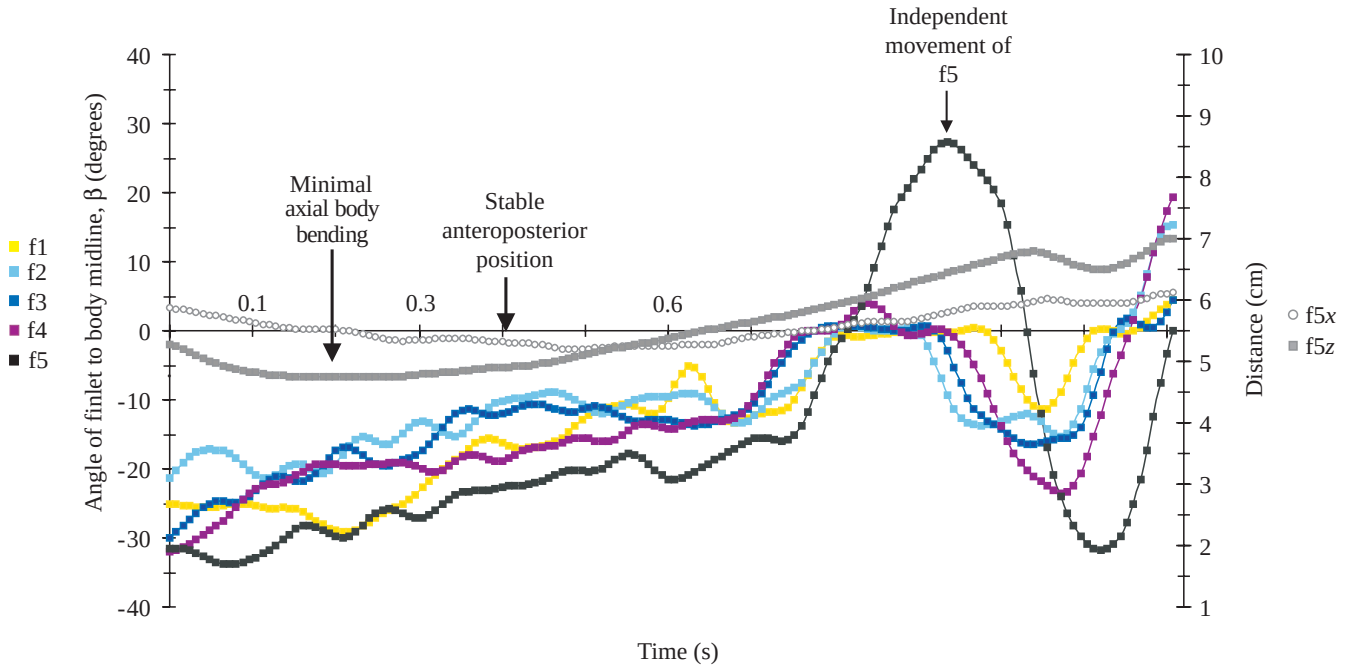

Fig. 8. The angle of the finlets relative to the body midline (β) of a 22 cm fish gliding (indicated by minimal axial body bending finlet 5; gray squares) at a constant speed (indicated by the stable anteroposterior position of finlet 5; open circles) of 0.85 $L\,s^{-1}$, where L is fork length.

individual×finlet effects (Table 2). *Post-hoc* tests indicated that the magnitudes of the vertical (*y*) excursion of finlets 3 and 4 were significantly different from that of finlet 5 (Fig. 7B). The excursion magnitudes of all three finlets were significantly different from each other in both the *x* and *z* directions (Fig. 7A,C). Although a MANOVA could not be performed on the excursion data because of insufficient degrees of freedom, it is apparent that, in terms of absolute distance, the *z* excursions were dominant (Fig. 7C). For the three fish examined, finlet 5 was approximately 12 mm in length (mean ± S.D.=12.4±2.5 mm). On average, the maximal *z* excursions of finlet 5 were approximately 5 mm (Fig. 7C) compared with maximal excursion values of approximately 3 mm and 2.5 mm for the *x* and *y* planes, respectively (Fig. 7A,B).

Finlet kinematics during gliding

The 22 cm individual swimming at less than 1 $L\,s^{-1}$ often glided for more than a second between tailbeats while maintaining a steady position in the flow. During gliding, the finlets sometimes remained motionless, and a finlet would subsequently move independently of both body undulation and the movement of any other finlets (Fig. 8). In the case shown here, finlet 5 shows independent movement. Its maximum amplitude of oscillation (β=28 °) at the fish's speed of 0.85 $L\,s^{-1}$ is similar to that seen for finlet 5 at swimming speeds up to 3.0 $L\,s^{-1}$ (Figs 5, 6A).

Angle of attack (α)

An ANOVA of the α data as a function of tail position (at mid-stroke or at the stroke extreme), structure (finlets 3, 4 or 5 or the tail) and individual, indicated that the data showed significant effects from structure (P<0.0002), individual (P<0.0001) and tail position×structure (P<0.0141, Table 3). The significant tail position×structure effect indicates that the effect of the position of the tail on α values was different for the different finlets and the tail. *Post-hoc* tests indicated that the α_{tail} values were significantly different from all the α_{finlet} values, which were not significantly different from each other.

The data in Fig. 9 illustrate these statistical results. During steady swimming at 2.2 $L\,s^{-1}$, α_{tail} values oscillated rapidly from minimum values of −14 ° to maximum values of 33 ° as the tail moved through a stroke. As the caudal peduncle crossed the body midline, values of α_{tail} were high (17±6 °, mean ± S.D., N=6). Maximum values of α_{tail} occurred after the caudal peduncle had crossed the body midline (phase lag 18±4 % of the cycle, mean ± S.D., N=6). As the caudal peduncle approached maximum excursion, values of α_{tail} decreased rapidly (to −3±4 °; mean ± S.D., N=28).

In contrast, the angles of attack of finlets 3, 4 and 5 (α_{finlet})

Table 3. *Results (F-values) of the two-way ANOVAs on the angle of attack (α) of finlets 3, 4, 5 and the tail (the structure effect) at mid-stroke and at the extreme of a stroke*

Variable	Individual	Structure	Tail position × structure
d.f.	2, 126	3, 6	3, 126
α	11.1	39.3	8.5

d.f. is the degrees of freedom.

Only the statistically significant (P<0.05) effects and interactions are shown.

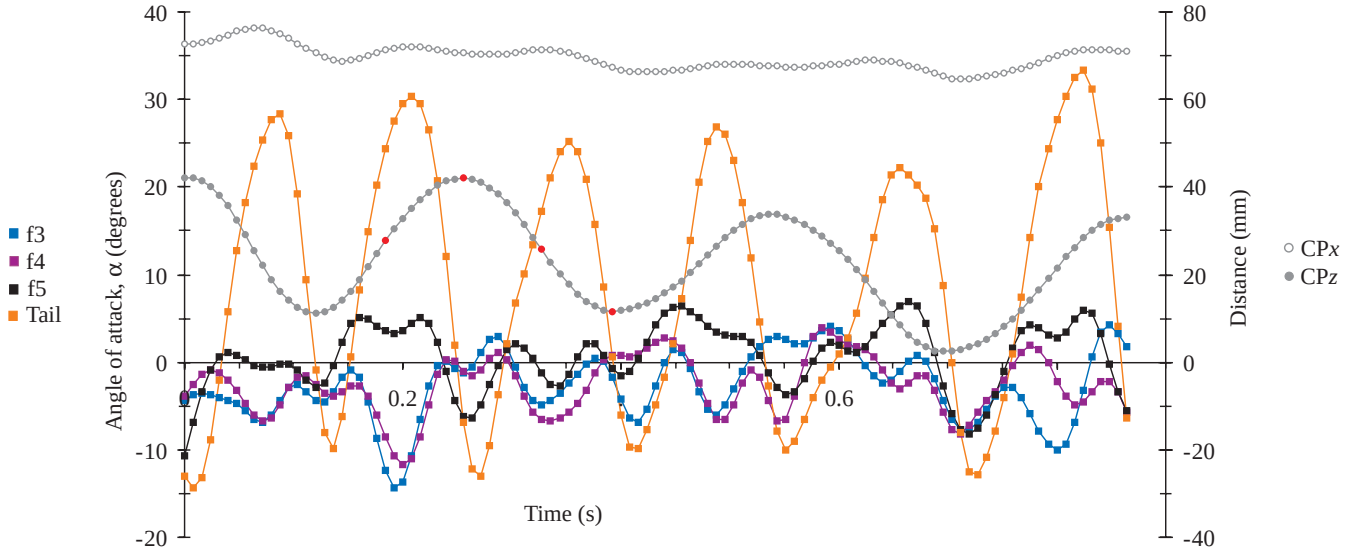

Fig. 9. A time series of the angle of attack (α) of finlets 3 (f3, blue), 4 (f4, purple) and 5 (f5, black) and the tail (orange), and the *x* (gray circles) and *z* (gray squares) positions of the caudal peduncle (CP) of a 19 cm fish swimming at 2.2 *L* s^{-1}, where *L* is fork length. The four red symbols indicate time points for which α data are plotted as a function of the animal's path of motion in Fig. 10.

were variable and showed no clear pattern in relation to caudal peduncle movement. As the caudal peduncle crossed the midline of the body, α_{finlet} values tended to be low (–2±5°, mean ± S.D., *N*=18). The lack of change in α_{finlet} over the tailbeat contrasts with the pattern seen in α_{tail}; this difference resulted in the significant effect of tail position×structure in the ANOVA (Table 3). Over these three tailbeats, α_{tail} averaged 9±14° (mean ± S.D., *N*=107); average values of α_{finlet} were –3±1°, –3±2° and –1±4° for finlets 3, 4 and 5 respectively (means ± S.D., *N*=107).

To illustrate α as a function of the fish's movement, the path of motion of the caudal peduncle from the time series data in Fig. 9 is plotted in Fig. 10. Outlines of the dorsal view of the fish with the position and values of α for finlets 3–5 and the tail are shown for four time points (indicated by the red symbols in Fig. 9). This tailbeat was 0.312 s in duration; at the swimming speed of 2.2 *L* s^{-1}, the equivalent forward distance for this tailbeat was approximately 13 cm. The amplitude of lateral oscillation of the caudal peduncle was approximately 10 % of the distance traveled. Values of α_{tail} oscillated between

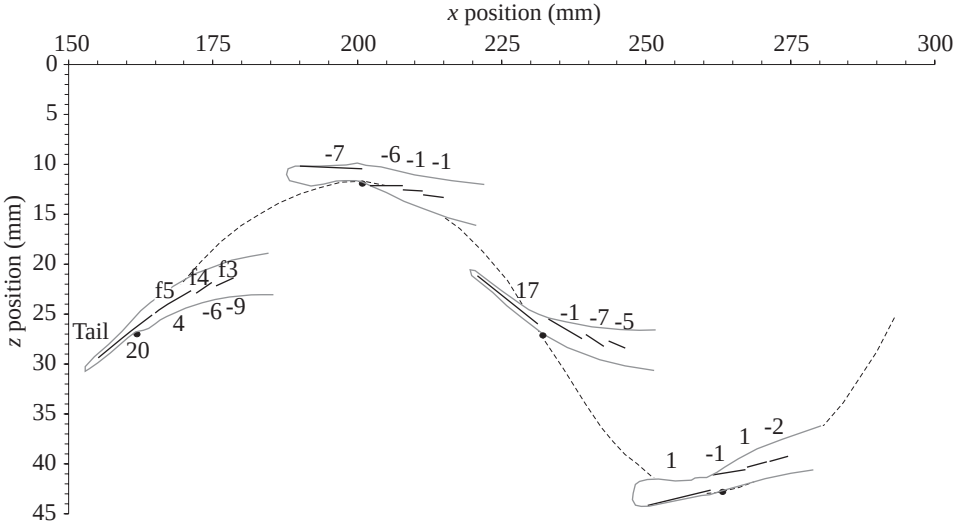

Fig. 10. The angle of attack (α) and position of finlets 3, 4, 5 (f3, f4 and f5) and the tail for a 19.1 cm fish swimming at 2.2 *L* s^{-1}, where *L* is fork length. These data are a subset of the data in Fig. 9; red markers in that time series indicate the time points of the four images. The dashed line is the path of motion of the caudal peduncle for one tailbeat that lasted 0.312 s. The outline of the dorsal view of the fish is the gray solid line. The black solid lines indicate the positions of finlets 3, 4 and 5 and the dorsal margin of the tail. The numbers associated with each finlet and the tail are the α values at that moment; the α values were calculated using image pairs 0.008 s apart in time. The black dot on each outline is the point on the caudal peduncle digitized for an index of body movement.

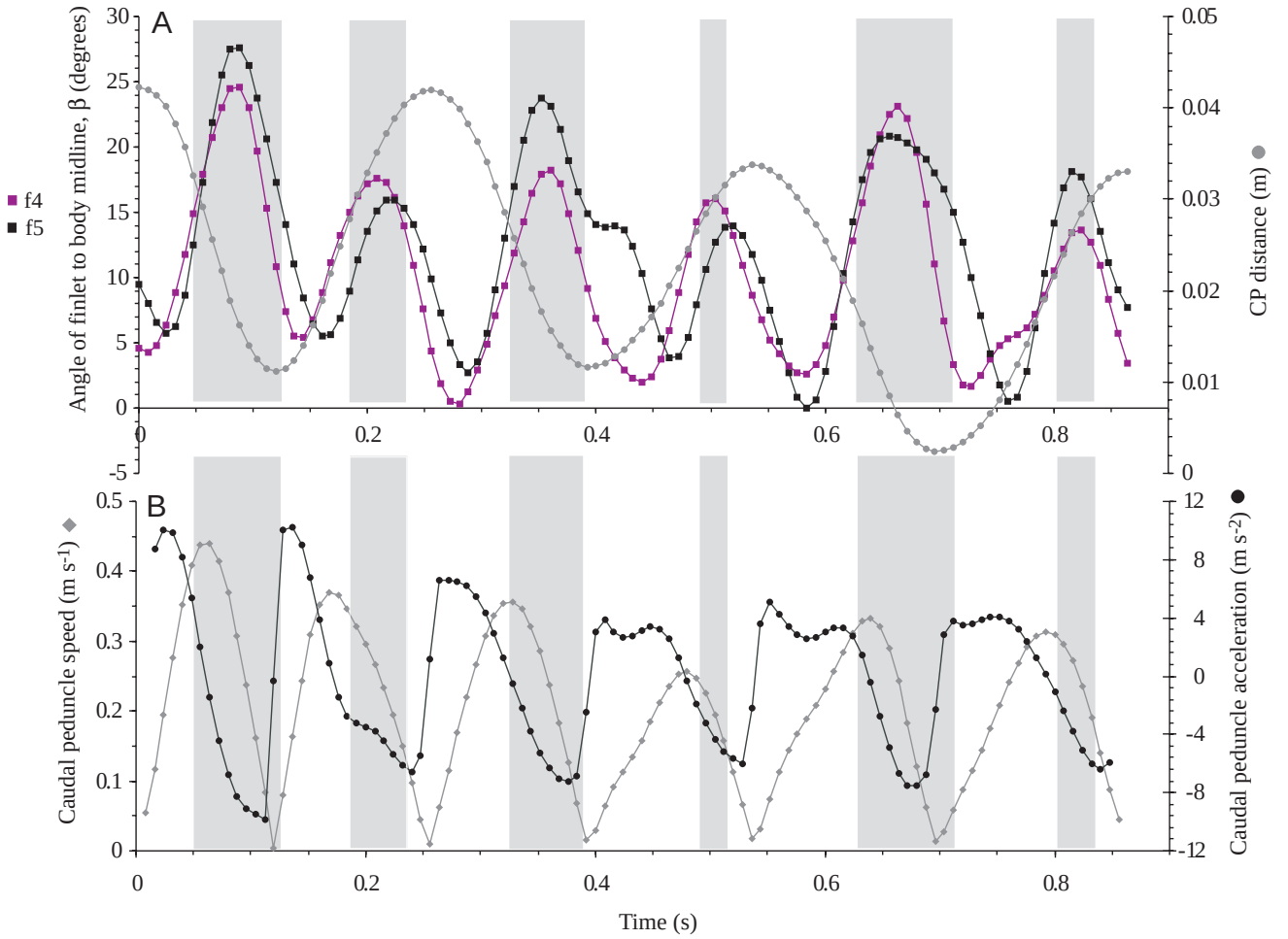

Fig. 11. A time series of the angle between finlets 4 (f4, purple squares) and 5 (f5, black squares) and the body midline (β, A) and the distance (gray circles, A), speed (gray triangles, B) and acceleration (black circles, B) of the caudal peduncle (CP). As an index of large finlet excursions, the highlighted areas indicate the times at which the β values for finlet 4 or finlet 5 are greater than 15 °.

20 and −7 °, with high positive values mid-beat (over this tailbeat α_{tail}=9±14 °, mean ± S.D., *N*=37). Values of α_{finlet} were mostly negative (over this tailbeat α_{finlet}=−2±4 °, mean ± S.D., *N*=111), indicating that the finlets were not contributing to thrust production.

Plotting the β values of finlets 4 and 5 for this time series with calculations of the speed and acceleration of the caudal peduncle (Fig. 11) shows that, for finlets 4 and 5, high values of β generally coincide with the deceleration of the tail. By definition, when β is high, the *x* and *z* excursions of the finlet are also high. Video data show that the *y* excursion of the finlet is also high at this time. This indicates that finlet excursion is high as the tail is decelerating. At this time of high excursion, the finlets could be directing some of their local flow longitudinally (Fig. 12), which could strengthen the vortex forming at the tail.

Discussion

Finlet structure and kinematics in Scomber japonicus

The morphological data presented here offer several insights into the potential locomotory role of the finlets. Summed finlet area is approximately 15 % of the surface area of the caudal fin. Thus, the finlets represent a significant additional lateral surface for interaction with the water, which may increase with growth relative to body surface area given the slight positive allometry of finlet length, height and area. The posterior increase in finlet size, and concurrent tapering of the body towards the caudal fin, results in the largest finlets positioned at the narrowest part of the body, i.e. just anterior to the tail. This suggests that the more posterior finlets will have a larger effect than the anterior finlets on both their immediate flow environment and the hydrodynamics of the caudal fin. Interestingly, the most posterior finlet is unique in its morphology. Its double-finlet structure results in increased finlet length and a tendency for increased surface area; both variables will affect water flow near the tail.

The observation that the timing, amplitude and phase of maximum finlet excursion were all independent of speed during steady swimming over a range of 1.2–3.0 $L\,s^{-1}$ (Fig. 6) indicates that at speeds above 1.0 $L\,s^{-1}$ finlet movement is largely passive. The finding that averaged over a tailbeat the

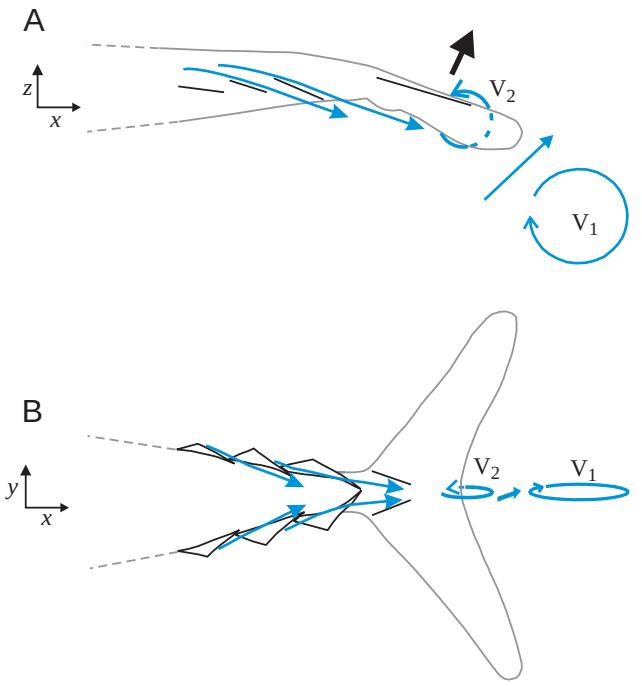

Fig. 12. A vorticity enhancement hypothesis of finlet function during locomotion: (A) dorsal view; (B) lateral view. The mackerel body outline is shown in gray and the finlets are shown in black (following the convention of Fig. 10). One possible path of water flow over the finlets is indicated in blue. Both views show the tail at the time it is decelerating towards the end of a beat to the fish's right. Water flowing over the caudal peduncle may be directed by finlets into the developing vortex V_2. Addition of relatively high-velocity flow to the vortex would enhance vorticity and circulation and, hence, enhance thrust. V_1, shed vortex.

angle of attack (α) values for finlets 3–5 are approximately zero (Fig. 9) also indicates that finlet movement is largely passive. Thus, at speeds above $1.0\,L\,s^{-1}$, finlet movement is probably largely dictated by the water flow around the fish and by any anatomical limitations to movement at the anterior base of each finlet, such as the structure of the articulation, the connective tissue or the muscle insertions at the attachment of the finlet fin rays to the cartilaginous pad (Fig. 2C).

Instantaneous α values of the finlets as high as 5° and as low as –10° (Fig. 9), however, preclude a definitive conclusion that finlet movement is passive at swimming speeds commonly used for cruising. These α values suggest that there is some instantaneous control of finlet movement. Finlet movement may, therefore, result from a combination of active and passive effects, the relative proportion of which may change with speed. For example, the muscle fibers attaching to the finlet base could be activated at all swimming speeds, but be largely unable to overcome forces exerted by the fluid on each finlet. Planned future electromyographic experiments on finlet muscles and nearby myotomal fibers will provide additional data to evaluate the extent to which finlet motion is under active control during steady swimming.

Active control of finlet movement was demonstrated during gliding at low, steady speeds by the movement of a finlet independent of body undulation and the movement of other finlets (Fig. 8). The fact that a period of inactivity of all finlets was followed by a period of activity of a single finlet indicates that the movement was actively controlled, because a passive response to flow would probably be shown in more than one finlet at a time. Such movements of the finlets often resulted, after a delay, in a slight repositioning of the body in the flow. It is possible that the independent movements of finlets during gliding at low speeds are small 'steering' corrections and serve to change the orientation of the body prior to the next set of active tailbeats. This hypothesis can be tested with flow visualization experiments at low speeds to determine whether the finlets deflect fluid passing over the peduncular region during gliding and how this may relate to subtle reorientation of the body after finlet movement.

Finlets could possibly also serve to provide sensory feedback on patterns of water flow in the region anterior to the tail. Proprioceptors in the connective tissue at the base of the finlets or around finlet muscles, similar to those reported in other specialized structures in fishes (Ono, 1979; Ono and Poss, 1982), could provide information on the gross characteristics of flow that might then be used to alter myotomal activity patterns and tailbeat kinematics. As fluid flowing over finlet 5 will have passed the tail in 20 ms (in fish of the size studied here swimming at $2\,L\,s^{-1}$), however, no compensatory kinematic modulation could occur unless the gross characteristics of the flow were relatively long in duration compared with the duration of a single tailbeat (approximately 300 ms).

Hydrodynamic role of the finlets

The position of the finlets immediately anterior to the tail suggests that they are a factor in swimming mechanics. The summed surface area of the finlets is approximately 15% of the caudal fin area, suggesting that the finlets could produce a significant amount of thrust during steady swimming. The angle of attack (α) values of the finlets were generally low and showed no clear pattern of change relative to the tail, however, so the data indicate that the finlets are not contributing to thrust production *via* classical lift-based mechanisms. Note that the α calculations were based on an assumption that the flow local to a finlet or the tail is approximated by the path of movement of that structure. We are currently testing this hypothesis with digital particle image velocimetry (DPIV) methods previously used for studies of pectoral fin function (Drucker and Lauder, 1999; Wilga and Lauder, 1999).

Non-retractable fins positioned adjacent to the caudal peduncle, such as the adipose fin of the sockeye salmon *Oncorhynchus nerka*, have been proposed to help control turbulence in the cross-flow over the caudal peduncle by, for example, generating microturbulence (Wardle, 1977). Given their position on the body, the finlets probably affect cross-flow over the caudal peduncle. The angle of attack data indicated that finlet movement in the *x*,*z* plane is largely passive at normal cruising speeds. However, these relatively stiff structures may

act as a baffle and thus dampen turbulence in the cross-flow. Cross-flow turbulence would presumably be a more important factor for schooling fish than for solitary animals.

Aleev (1969) and Helfman et al. (1997) hypothesized that the finlets eliminate or prevent vortices in water shed from the median fins and thus provide a less turbulent environment for oscillation of the tail. Given the relatively small height of each finlet relative to the second dorsal and anal fins and the caudal fin, and the tapering of the body posterior the second dorsal fin, it seems unlikely that the finlets have a large effect on any vortices shed anteriorly to them or on the general flow environment of the entire caudal fin.

Longitudinal deflection of water by the finlets has been proposed by Walters (1962), Lindsey (1978) and Magnuson (1970). The present kinematic data also suggest that the finlets may deflect water longitudinally. At maximum excursion, the finlets are deflected laterally and vertically. In particular, the fifth finlet undergoes a large vertical deflection so that the tips of dorsal and ventral finlet 5 actually meet on the side of the fish (depicted in Fig. 12B). It seems likely that at this orientation the most posterior finlets could deflect water longitudinally along the body. It is noteworthy that, on the basis of the orientation of the posterior finlets, we predict that fluid will be directed along the peduncle in the region of the two caudal keels (Figs 2C, 12B), which themselves have been hypothesized to accelerate flow into the caudal fin region (Collette, 1978).

Magnuson (1970) proposed that longitudinally directed flow would augment lift forces produced at the large, external central caudal keel of *Euthynnus affinis*. This hypothesis is unlikely to apply to *Scomber japonicus* given its lack of an external central keel and relatively low-profile lateral keels. Longitudinally directed flow may slow boundary layer separation and thus reduce drag (Lindsey, 1978). This hypothesis could be tested by imaging the boundary layer flow on a fish before and after finlet removal. Alternatively, the data presented here on the timing of finlet movement relative to tail motion suggest an alternative, interesting possibility for thrust enhancement by the finlets. The finlets reach their maximum lateral excursion as the tail is decelerating during the second quarter of the tailbeat to one side (Fig. 11). Flow directed across the caudal peduncle into the midline of the tail could add momentum to the center of the vortex forming at the tail (V_2 in Fig. 12). The addition of relatively high-velocity fluid to the developing vortex will increase circulation and thus increase net thrust.

This vortex enhancement hypothesis suggests that at the time of maximum excursion one would see a longitudinally directed flow over the finlets and along the caudal peduncle. In addition, the reasoning presented above suggests that the vortex rings from an intact individual of *Scomber japonicus* will be larger than those from that individual with its finlets removed (given the same swimming speed). This hypothesis can also be tested using DPIV, assuming that there is a very high repeatability in caudal fin vortex ring characteristics from individuals swimming at a steady speed. In addition, a high level of precision will be required in the measurement techniques used to characterize vortex strength because the effect of the finlets on hydrodynamic efficiency is likely to be relatively small. For example, a net increase in thrust of the order of 1–5 % would be advantageous to the continuously swimming mackerel, but may be difficult to measure in the laboratory.

Finlets in other fishes

Finlets are not a unique characteristic of scombrids. For example, the sauries (Scomberesocidae), four marine epipelagic species found in tropical and temperate waters, have 5–7 finlets situated posterior to both the dorsal and anal fins (Nelson, 1984). The snake mackerels (Gempylidae) are found in marine, tropical and subtropical seas, often in deep water, and have what are described as ‘isolated finlets’ behind the dorsal and anal fins (Nelson, 1984). Essentially nothing is known about the kinematics or hydrodynamics of these species. In addition, although outgroup taxa such as billfishes lack finlets, some species (such as the Atlantic blue marlin *Makaira nigricans*) show second dorsal and anal fins with finlet-like shapes (a roughly triangular morphology with a long tapering ventral margin extending posteriorly). Finally, the reduced adipose fin of, for example, the Salmoniformes, is grossly similar in shape and position to a finlet. More experiments are necessary to determine the hydrodynamic significance (if any) of this recurring morphological design.

The authors gratefully acknowledge Bob Shadwick, Scott Rapoport, Harry Helling and Jimmy Liao for assistance in obtaining and housing the mackerel for this study. Chris Gaetano, Eliot Drucker and Michelle Riele provided assistance during the experiments and/or during data analysis. We also thank Jimmy Liao, Cheryl Wilga, Lara Ferry-Graham, Eliot Drucker and Frank Fish for helpful comments during the course of this project. This manuscript was improved by comments from two anonymous referees. Support was provided by NSF grant 9807021 to G.V.L.

References

Aleev, Y. G. (1969). *Function and Gross Morphology in Fish*. Jerusalem: Keter Press. 268pp.

Beamish, F. W. H. (1978). Swimming capacity. In *Fish Physiology*, vol. VII, *Locomotion* (ed. W. S. Hoar and D. J. Randall), pp. 101–189. New York: Academic Press.

Biewener, A. A. and Full, R. J. (1992). Force platform and kinematic analysis. In *Biomechanics (Structures and Systems): A Practical Approach* (ed. A. A. Biewener), pp. 45–73. Oxford: Oxford University Press.

Blake, R. W., Chatters, L. M. and Domenici, P. (1995). Turning radius of yellowfin tuna (*Thunnus albacares*) in unsteady swimming manoeuvres. *J. Fish Biol.* **46**, 536–538.

Block, B. A., Finnerty, J. R., Stewart, A. F. R. and Kidd, J. (1993). Evolution of endothermy in fish: mapping physiological traits on a molecular phylogeny. *Science* **260**, 210–214.

Collette, B. B. (1978). Adaptations and systematics of mackerels and

tunas. In *The Physiological Ecology of Tunas* (ed. G. D. Sharp and A. E. Dizon), pp. 7–39. New York: Academic Press.

Collette, B. B. and Nauen, C. E. (1983). *Scombrids of the World. FAO Species Catalogue 125*, vol. 2. Rome: Food and Agriculture Organization of the United Nations. 137pp.

Davis, J. C. (1986). *Statistics and Data Analysis in Geology*. New York: John Wiley & Sons. 646pp.

Dewar, H. and Graham, J. B. (1994). Studies of tropical tuna swimming performance in a large water tunnel. III. Kinematics. *J. Exp. Biol.* **192**, 45–59.

Dingerkus, G. and Uhler, L. D. (1977). Enzyme clearing and staining of alcian blue stained whole small vertebrates for demonstration of cartilage. *Stain Technol.* **52**, 229–232.

Drucker, E. G. and Lauder, G. V. (1999). Locomotor forces on a swimming fish: three-dimensional vortex wake dynamics quantified with digital particle image velocimetry. *J. Exp. Biol.* **202**, 2393–2412.

Fierstine, H. L. and Walters, V. (1968). Studies in locomotion and anatomy of scombroid fishes. *Mem. S. Calif. Acad. Sci.* **6**, 1–31.

Gibb, A. C., Dickson, K. A. and Lauder, G. V. (1999). Tail kinematics of the chub mackerel *Scomber japonicus*: testing the homocercal tail model of fish propulsion. *J. Exp. Biol.* **202**, 2433–2447.

Gillis, G. B. (1997). Anguilliform locomotion in an elongate salamander (*Siren intermedia*): effects of speed on axial undulatory movements. *J. Exp. Biol.* **200**, 767–784.

Helfman, G. S., Collette, B. B. and Facey, D. E. (1997). *The Diversity of Fishes*. Malden: Blackwell Scientific. 528pp.

Jayne, B. C., Lozada, A. F. and Lauder, G. V. (1996). Function of the dorsal fin in bluegill sunfish: motor patterns during four distinct locomotor behaviors. *J. Morph.* **228**, 307–326.

LaBarbera, M. (1989). Analyzing body size as a factor in ecology and evolution. *Annu. Rev. Ecol. Syst.* **20**, 97–117.

Lindsey, C. C. (1978). Form, function and locomotory habits in fish. In *Fish Physiology*, vol. VII, *Locomotion* (ed. W. S. Hoar and D. J. Randall), pp. 1–100. New York: Academic Press.

Magnuson, J. J. (1970). Hydrostatic equilibrium of *Euthynnus affinis*, a pelagic teleost without a gas bladder. *Copeia* **1**, 56–85.

Magnuson, J. J. (1978). Locomotion by scombrid fishes: hydromechanics, morphology and behavior. In *Fish Physiology*, vol. VII, *Locomotion* (ed. W. S. Hoar and D. J. Randall), pp. 239–313. New York: Academic Press.

Nauen, J. C. and Shadwick, R. E. (1999). The scaling of acceleratory aquatic performance: body size and tail flip performance of the California spiny lobster *Panulirus interruptus*. *J. Exp. Biol.* **202**, 3181–3193.

Nelson, J. S. (1984). *Fishes of the World.* New York: John Wiley & Sons. 523pp.

Ono, R. D. (1979). Sensory nerve endings of highly mobile structures in two marine teleost fishes. *Zoomorph.* **92**, 107–114.

Ono, R. D. and Poss, S. G. (1982). Structure and innervation of the swim bladder in the weakfish, *Cynoscion regalis* (Teleostei: Sciaenidae). *Can. J. Zool.* **60**, 1955–1967.

Walker, J. A. (1998). Estimating velocities and accelerations of animal locomotion: a simulation experiment comparing numerical differentiation algorithms. *J. Exp. Biol.* **201**, 981–995.

Walters, V. (1962). Body form and swimming performance in the scombroid fishes. *Am. Zool.* **2**, 143–149.

Wardle, C. S. (1977). Effects of size on the swimming speeds of fish. In *Scale Effects in Animal Locomotion* (ed. T. J. Pedley), pp. 299–313. New York: Academic Press.

Wardle, C. S. and He, P. (1988). Burst swimming speeds of mackerel, *Scomber scombrus* L. *J. Fish Biol.* **32**, 471–478.

Westneat, M. W., Hoese, W., Pell, C. A. and Wainwright, S. A. (1993). The horizontal septum: mechanisms of force transfer in locomotion of scombrid fishes (Scombridae, Perciformes). *J. Morph.* **217**, 183–204.

Wilga, C. D. and Lauder, G. V. (1999). Locomotion in sturgeon: function of the pectoral fins. *J. Exp. Biol.* **202**, 2413–2432.

Winter, D. A. (1989). *Biomechanics and Motor Control of Human Movement.* New York: John Wiley & Sons, Inc.

Yuen, H. S. H. (1970). Behavior of a skipjack tuna, *Katsuwonus pelamis*, as determined by tracking with ultrasonic devices. *J. Fish. Res. Bd Can.* **27**, 2071–2079.

Zar, J. H. (1984). *Biostatistical Analysis*. Englewood Cliffs: Prentice Hall. 718pp.